17 Local Distribution Approach

Andreas Alvermann and Holger Fehske

Institut für Physik, Universität Greifswald, 17487 Greifswald, Germany

In this contribution we describe a stochastic approach to the analysis of random spatial fluctuations and accompanying correlation phenomena like Anderson localization. We first elucidate the basic conceptual ideas which motivate the use of distributions of local Green functions in this approach, and then present details of the technique and its implementation. We illustrate its application by examples taken from the field of disordered solids. The inclusion of interaction by means of dynamical mean-field theory then is a possible starting point for a unified treatment of disorder and interaction.

17.1 Introduction

Any theory of condensed matter – at least a proper quantum mechanical one – has to include spatial and temporal fluctuations, and the correlations that develop between these. Fluctuations in time naturally arise in any interacting system, where a particle can exchange energy with the rest of the system. In a number of situations spatial fluctuations are equally important. As we learn in the Born-Oppenheimer approximation [1], electrons in a solid see the ions mainly through a static potential. In disordered systems spatial fluctuations then arise from an irregular arrangement of the ions. Even for a regular crystal, at finite temperature ions are elongated from their equilibrium positions, and the ionic potential fluctuates in space. On a technical level, the Hubbard-Stratonovich transformation [2, 3] shows how an interacting fermion system can be mapped onto a non-interacting one coupled to auxiliary fields which fluctuate in space (and time).

In traditional mean-field descriptions, such as the Weiss theory of magnetism, fluctuations are at best approximately described, if not neglected at all. As a major improvement the dynamical mean-field theory (DMFT) [4] – for a detailed explanation and a list of references we refer the reader to Chap. 16 – includes fluctuations and correlations in time by establishing a self-consistent theory for a local but energy-dependent interaction self-energy. In the course of the DMFT construction, which is based on the limit of infinite dimension ($d = \infty$), spatial fluctuations are averaged out. A natural question is whether one can set up a kind of mean-field theory which accounts for fluctuations and correlations in space. This contribution will try to explain that an affirmative answer can be found if one adopts a viewpoint which has been first advocated for by P. W. Anderson in developing his theory of

A. Alvermann and H. Fehske: *Local Distribution Approach*, Lect. Notes Phys. **739**, 505–526 (2008)
DOI 10.1007/978-3-540-74686-7_17

localization in disordered systems [5]: To take the stochastic nature of spatial fluctuations serious. Then quantities like the density of states become site-dependent random quantities, and one has to deal with their distribution instead of some averages.

In this tutorial we are going to describe an approach resting on this stochastic viewpoint. This approach employs the distribution of the local density of states as the quantity of interest, and is accordingly denoted as local distribution (LD) approach. We will explain how to turn this approach into a working method, and apply it to two important examples of disordered non-interacting systems. In the discussion of the results we will relate it to a method based on averages, the coherent potential approximation (CPA) [6]. Then we outline how to combine the stochastic approach with DMFT to address both interaction and disorder. Anderson localization of a Holstein polaron serves as a particular example in this context. Finally, we take a short look how to cast the Holstein model at finite temperature into a stochastic framework. There is one word of warning to the reader: What we are going to explain is a fully worked out machinery only to a lesser degree, but constitutes an original way of thinking which has yet found some applications. This tutorial will hopefully serve the purpose to get the reader accustomed to the fundamental concepts of a stochastic approach to spatial fluctuations, and to convince him that the stochastic viewpoint is essential for an appropriate treatment.

17.1.1 Basic Concepts

We can present the basic ideas best if we concentrate on disordered systems, where spatial fluctuations are explicitly imposed.[1] In a substitutionally disordered system, like a doped semiconductor or an alloy, disorder primarily manifests through site-dependent random potentials ϵ_i. A model to describe electron motion in such a disordered crystal is given by

$$H = \sum_i \epsilon_i c_i^\dagger c_i - t \sum_{\langle i,j \rangle} c_i^\dagger c_j \ . \tag{17.1}$$

In this Hamiltonian, $c_i^{(\dagger)}$ denote fermionic operators for tight-binding electrons on a crystal lattice, and the ϵ_i account for local potentials arising from the ions composing the crystal. Note that this is a model of non-interacting fermions whose non-trivial properties arise from the randomness present in ϵ_i. Due to randomness, the ϵ_i are not fixed to some concrete values, but only their range of possible values is specified by a probability distribution $p(\epsilon_i)$. Two examples, which will be discussed below in detail, are the binary alloy with $p(\epsilon_i) = c_A \delta(\epsilon_i + \Delta/2) + (1 - c_A)\delta(\epsilon_i - \Delta/2)$, and the Anderson model of localization $p(\epsilon_i) = (1/\gamma)\,\Theta(\gamma/2 - |\epsilon_i|)$ (see (17.9) and (17.10)).

A material of certain composition corresponds to some $p(\epsilon_i)$, while any single specimen of this material is described by choosing values for ϵ_i according to $p(\epsilon_i)$.

[1] For reviews on the interesting physics of disordered systems we refer the reader to [7, 8].

Any $p(\epsilon_i)$ therefore defines many Hamiltonians (17.1), one for each concrete choice of all $\{\epsilon_i\}$. Any experiment is carried out on a single specimen, i.e. one of these Hamiltonians, while in generally we want to describe common properties of all Hamiltonians defined by $p(\epsilon_i)$. How then is the *typical* behavior for some $p(\epsilon_i)$ related to the *specific* behavior for fixed ϵ_i? For any finite system, there is a small chance to find untypical values for $\{\epsilon_i\}$. For the binary alloy (see (17.9) below) for example, there is a finite probability $c_A^N + c_B^N$ to have all ϵ_i equal on N sites – which gives an ordered system with untypical behavior for the disordered one. In a crystal with many sites however, this probability is vanishingly small: In this sense any disordered specimen is typical for the material class.[2]

In a disordered system translational invariance is broken. In contrast to the description of ordered systems we then employ quantities that depend on position, like the local density of states (LDOS) $\rho_i(\omega)$. The LDOS counts the number of states at a certain energy ω at lattice site i. It is related to the local Green function $G_{ii}(\omega) = \langle i|(\omega - H)^{-1}|i\rangle$ by

$$\rho_i(\omega) = -\,\mathrm{Im}\;\, G_{ii}(\omega)/\pi\;. \tag{17.2}$$

From the LDOS the density of states (DOS) $\rho(\omega)$ is obtained as the average over the crystal volume, $\rho(\omega) = \frac{1}{N}\sum_i \rho_i(\omega)$ for an N-site lattice. The LDOS generally contains more information than the DOS. Only in absence of disorder, $\rho_i(\omega) = \rho(\omega)$ for all i. But with disorder, $\rho_i(\omega)$ fluctuates through the system. The important point we will discuss later is that it would be wrong to say that the LDOS fluctuates *around* the DOS. In generally, LDOS fluctuations can render the concept of an averaged DOS to described the system in whole almost useless.

A tool to measure the LDOS in the laboratory is scanning tunneling microscopy (STM). In STM, the tunneling current between a tip and the surface of a specimen is measured. The tunneling current is, in a suitable approximation, proportional to $\rho_i(\omega)$, convoluted with some apparatus function which accounts for the finite energy resolution of the STM device. For a given applied voltage STM can therefore produce a spatially resolved picture of the LDOS. Note that due to the finite energy resolution several states contribute to the picture of $\rho_i(\omega)$: One always measures the typical behavior of some eigenstates of the Hamiltonian in the vicinity of ω.

What could not be done with STM, can be done by numerical techniques: To measure the LDOS even inside a three dimensional cube (Fig. 17.1). The computer first generates $N = L^3$ values for the ϵ_i in (17.1) using a random number generator, and then calculates the LDOS for L^2 sites in a quadratic slice of the cube using e.g. the kernel polynomial method (KPM) (see Chap. 19 in this book). Taking this

[2] The critical reader might note that this is not the more difficult question whether all quantities are self-averaging, that is mean and typical values coincide for large system sizes. The latter is true if the distribution of a quantity is sharp or at least peaked at the mean value. As e.g. the distribution $P[\rho_i(\omega)]$ of the local density of states shows, this is in general not the case. Whether it is true for the conductivity is a different question. The distribution of a quantity itself is nevertheless always typical.

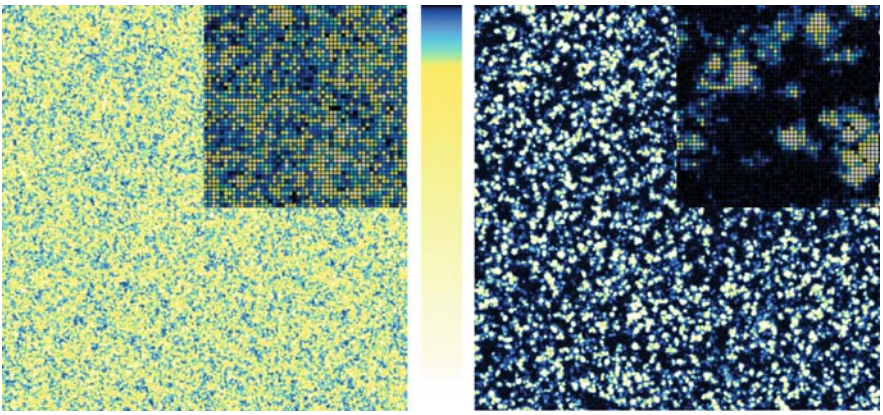

Fig. 17.1. LDOS $\rho_i(\omega)$ for a disordered cube of $N = L^3$, $L = 512$, sites. The values of ϵ_i were obtained according to the disorder distribution (17.10) of the Anderson model, with $\gamma/t = 10.0$, the calculation has been performed for periodic boundary conditions to avoid boundary effects. The pictures show a slice of L^2 sites, the value of $\rho_i(\omega)$ is color-coded, from black for very small to white for very large values (see color bar in the middle). In the upper right edge the 50^2 sites in the upper left edge of the picture are shown in magnification. Left: At energy $\omega/t = 0.0$, the LDOS is comparable throughout the crystal. Right: At $\omega/t = 7.69$, the LDOS is concentrated in finite, separated regions of the crystal. Evidently, the character of states is very different depending on energy. This indicates the existence of a phase transition, the so-called Anderson localization, which we will discuss in Sect. 17.2.1

picture,[3] one should easily accept that the site-dependence of the LDOS constitutes an eminent aspect of disordered systems. Apparently, the DOS is not significant for the different structure of the LDOS: On average, both LDOS pictures in Fig. 17.1 would look the same.

To account for the difference, we have to describe the fluctuations of the LDOS. Then, both LDOS pictures look different: The right one has strong fluctuations, most values being small but some very large, while in the left picture values are equally distributed in some range, and extreme values are rare. To quantify this behavior we can understand the LDOS with its different values at different sites as a statistical quantity, whose fluctuations are described by a distribution $P[\rho_i(\omega)]$. To construct the distribution from the explicit knowledge of the LDOS, we had to count how often the LDOS takes a value in a certain range. By this counting we would obtain $P[\rho_i(\omega)]$ as a histogram. Then, we could also recover the DOS as an (arithmetic) average

$$\rho(\omega) = \int_0^\infty \rho_i \, P[\rho_i(\omega)] \, \mathrm{d}\rho_i \; . \tag{17.3}$$

[3] With respect to the previous footnote, for $N = 512^3$ sites we expect that the LDOS shows typical behavior. Indeed, for two different sets of randomly generated values for the ϵ_i, the two pictures for the LDOS look qualitatively the same.

To find $P[\rho_i(\omega)]$ not only for one specific Hamiltonian out of the many given by (17.1) for a certain $p(\epsilon_i)$, we had to repeat this counting for many different choices of the ϵ_i until we get the typical form of $P[\rho_i(\omega)]$, which then no longer depends on concrete values of the ϵ_i but only on the disorder distribution $p(\epsilon_i)$. The aim of the stochastic approach is to construct this distribution at once.

Let us rethink the concept of the LDOS distribution, which we so far have introduced merely as a way of reorganizing information obtained from a calculation that does not mention distributions at all. To adopt the stochastic viewpoint entirely we must convince ourselves that distributions of observables are inherent in the definition of the model (17.1). Clearly, the Green function depends on all values $\{\epsilon_i\}$. Each of the values $G_{ii}(\omega;\{\epsilon_i\})$ occurs with the probability of the realization $\{\epsilon_i\}$, which is in turn given by the distribution $p(\epsilon_i)$. That is: The Green function by itself is a random variable right from the beginning, and we must deal with its distribution $P[G_{ii}(\omega)]$. As we will see this point of view is essential for the very understanding of disorder physics. We can now precisely formulate the task to be solved: To determine $P[G_{ii}(\omega)]$ from $p(\epsilon_i)$.

The distribution $P[G_{ii}(\omega)]$ has two important properties. First, though it clearly depends e.g. on energy ω, it does not depend on the lattice site i – remember, any value $G_{ii}(\omega;\{\epsilon_i\})$ for given $\{\epsilon_i\}$ does –, since due to the definition of model (17.1) each lattice site is equivalent. On the level of distributions we recover translational invariance which is otherwise lost. We keep the subscript i just to indicate a local Green function. Second, ergodicity implies a two-fold meaning of $P[G_{ii}(\omega)]$: It gives either the probability for a Green function value at a fixed lattice site but all possible $\{\epsilon_i\}$, or the probability for all lattice sites in a typical realization $\{\epsilon_i\}$. As we stated above, for an infinite lattice we get typical realizations almost surely.

17.1.2 Local Distribution Approach

We have yet advocated many times for using the distribution of the LDOS (or a Green function) instead of its average, the DOS. We now establish a scheme that provides us directly with the distribution for an infinite lattice. Since it is entirely formulated in terms of distributions of local Green functions, we call it local distribution (LD) approach.

For an arbitrary lattice, both the free DOS $\rho^0(\omega)$ and the connectivity K, i.e. the number of nearest neighbors, enter the LD equations. Compared to theories in the limit $d = \infty$, we have the additional parameter K. Since it is a bit tedious to establish the equations in the general case, we restrict to the case of a Bethe lattice (see Fig. 17.2) where we get simple equations straightforwardly, as has been first realized in [9]. As a byproduct, we obtain exact equations in this case. All principal physical features are retained despite this simplification, as we will demonstrate below.

The local Green function $G_{ii}(\omega)$ can always be expanded as

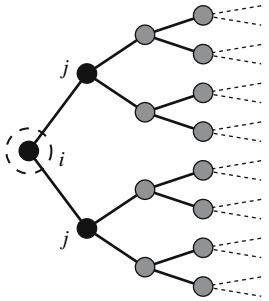

Fig. 17.2. Part of the half-infinite Bethe lattice for $K = 2$. The Bethe lattice is an infinite loop-free connected graph, where each site is connected to $K + 1$ different sites. Cutting one edge, we obtain the half-infinite Bethe lattice (or Bethe tree) as shown here. The relevance of Bethe lattices originates from the fact that a number of approximations become exact there – like the LD approach. However, the precise structure of the Bethe lattice is not as relevant for the LD approach as it may seem: In principle, only the free DOS is of importance. Especially simple equations are obtained for the Bethe lattice since the inverse Hilbert transform for the Bethe DOS is a simple, algebraic function

$$G_{ii}(\omega) = \left[\omega - \epsilon_i - t^2 \sum_{j,k=1}^{K} G_{jk}^{(i)}(\omega)\right]^{-1} . \tag{17.4}$$

Here, j, k run over all K neighbors of i, and the superscript (i) indicates that $G_{jk}^{(i)}(\omega)$ has to be calculated with site i removed from the lattice. On the Bethe lattice, no path connects different sites j, k adjacent to i once i has been removed. Accordingly, (17.4) simplifies to

$$G_i(\omega) = \left[\omega - \epsilon_i - t^2 \sum_{j=1}^{K} G_j(\omega)\right]^{-1} , \tag{17.5}$$

where $G_j(\omega)$ denotes the Green function $G_{jj}^{(i)}(\omega)$ where the site i to the left of j is removed (see Fig. 17.2).

Equation (17.5) contains only Green functions of the same type. Hence it is, in the absence of disorder ($\epsilon_i = 0$ for all i), a closed equation for the local Green function $G_i(\omega) = G_j(\omega)$. Solving that quadratic equation, we find the free Green function for the Bethe lattice with corresponding semi-circular density of states,

$$G_i^0(\omega) = \frac{8}{W^2}\left(\omega - \sqrt{\omega^2 - \frac{W^2}{4}}\right) , \tag{17.6}$$

$$\rho^0(\omega) = \frac{8}{\pi W^2}\sqrt{\frac{W^2}{4} - \omega^2} \qquad |\omega| \le \frac{W}{2} , \tag{17.7}$$

where $W = 4t\sqrt{K}$ is the bandwidth. Note that the DOS does not depend on K if W is fixed. In the limit $d = \infty$, for $K \to \infty$, the scaling $t \propto \widetilde{t}/\sqrt{K}$ keeps the bandwidth constant (cf. Chap. 16).

With disorder, the solution of (17.5) is less simple. Then, $G_i(\omega) \neq G_j(\omega)$, and (17.5) encodes an infinite set of coupled equations, depending on an infinite number of parameters $\{\epsilon_i\}$. The site-dependence of $G_i(\omega)$ prevents a closed equation for the local Green function, and hence a simple solution of the problem. But let us look at (17.5) once more from the stochastic viewpoint. We already know that the Green functions in this equation are random variables. We therefore find that (17.5) determines one random variable $G_i(\omega)$ from $K+1$ random variables ϵ_i and $G_j(\omega)$, $j = 1, \ldots, K$. We also know that $P[G_i(\omega)] = P[G_j(\omega)]$ for all j. Moreover the K Green functions $G_j(\omega)$ which appear on the r.h.s. of (17.5) are independently distributed. These two properties amount to read (17.5) as a self-consistency or fix-point equation for one random variable $G_i(\omega)$: It determines $G_i(\omega)$ on the l.h.s of (17.5) from K copies of $G_i(\omega)$ on the r.h.s. The on-site energy ϵ_i enters the equation as the source of randomness, parameterized by $p(\epsilon_i)$.

To explicitly state this essential point of the LD approach: By the stochastic reinterpretation of (17.5), the infinite set of equations for values of $G_i(\omega)$ turns out to be a single equation for the stochastic variable $G_i(\omega)$ (i.e., for its distribution $P[G_i(\omega)]$), with only one parameter $p(\epsilon_i)$. This amounts to a solution for $P[G_i(\omega)]$ entirely in terms of distributions, as provided by the sampling procedure described below.

For any finite K, (17.5) is a closed equation for the distribution of the random variable $G_i(\omega)$, which cannot be reduced to an equation for a single value like the average of $G_i(\omega)$. In the limit $d = \infty$ however, spatial fluctuations are averaged out, and (17.5) should simplify to one for averages then. Indeed, with the scaling $t \propto \widetilde{t}/\sqrt{K}$ for $K \to \infty$, the r.h.s. of (17.5) contains a sum of K summands multiplied with $1/K$. Hence this sum becomes an average for $K \to \infty$ according to the law of large numbers. Integrating over ϵ_i gives an average also on the l.h.s., and we obtain the equation

$$G^{\text{ave}}(\omega) = \int \left[\omega - \epsilon - \frac{W^2}{16} G^{\text{ave}}(\omega)\right]^{-1} p(\epsilon)\, \mathrm{d}\epsilon \tag{17.8}$$

for the disorder averaged Green function $G^{\text{ave}}(\omega)$. This equation is just the self-consistency equation of the so-called coherent potential approximation (CPA) for the Bethe lattice[4]. Since (17.5) is exact we have, for the special case of the Bethe lattice, proven that the CPA becomes exact for $K \to \infty$.

17.1.3 Monte Carlo Solution of the Stochastic Fix-Point Equation

It remains to solve the stochastic self-consistency equation (17.5) for $P[G_i(\omega)]$. We employ a sampling technique which is related to the Gibbs sampling method. Here

[4] For an extensive review on CPA see [6].

we have to deal with infinitely many random variables instead of finitely many as in standard Gibbs sampling.

Generally, the sampling solves any stochastic fix-point equation of the form $x = F[x, \ldots, x, \epsilon]$, where x and ϵ are random variables, $F[x_1, \ldots, x_K, \epsilon]$ is a function[5] that takes K values x_i of x and one value of ϵ. The distribution $p(\epsilon)$ of the external variable ϵ is known a priori. Obviously (17.5) is of that form, with $F[G_1, \ldots, G_K, \epsilon_i]$ given by the r.h.s. of the equation. Then, an implicit equation has to be solved: If one already knew the solution $P[x]$ one would obtain it again by means of $F[x, \ldots, x, \epsilon]$. Note the difference to the prominent Monte Carlo technique of importance sampling: While the latter one performs an integral with respect to a given known distribution, we have to construct the distribution from scratch. For that purpose we need to represent the distribution, which is conveniently done by a sample with a certain number N_s of entries x_i. Each entry will, as soon as the solution to the fix-point equation is obtained, be a possible value of x, and the fraction of entries in a certain range does determine $P[x]$. To read off $P[x]$ from the sample, we therefore construct a histogram by counting the appearances of entries in specified intervals; to build up a sample to $P[x]$ we throw N_s dice, weighted with $P[x]$, and take the N_s outcomes as sample entries. We note that any permutation of the sample still represents the same distribution.

The algorithm shown below solves the stochastic fix-point equation like one is tempted to solve any fix-point equation: By iteration. Starting with initial random values the sample is repeatedly updated until convergence is obtained. Then the distribution represented by the sample is a fix-point of the equation. To examine the following algorithm closely is a good way to comprehend the interpretation of (17.5) as a stochastic self-consistency equation.

```
input: distribution p(e), functional F, sample size Ns
output: sample and distribution for P[x]

(1) initialize sample S[i] with random data
(2) for i=1,Ns
   (2a) find random value for e
        using a random number generator for p(e)
   (2b) find random indices j[1],...,j[K] within 1,...,Ns
   (2c) calculate new value for S[i]=F[S[j[1]],...,S[j[K]],e]
(3) if notConverged goto 2

(4) construct distribution P[x] from S[i] as histogramm
(4') calculate averages of P[x] by summing over S[i]
```

We remind ourselves that convergence of the sample does not mean convergence of its entries but of the distribution represented. In practice, we may check this by comparison of some moments extracted of the distributions before and after each update `(2)`. In principle, convergence of the sampling algorithm cannot be

[5] For the equation to make sense, one requires $F[x_{\sigma_1}, \ldots, x_{\sigma_K}, \epsilon] = F[x_1, \ldots, x_K, \epsilon]$ for all permutations σ.

guaranteed, but depends on convergence of the non-stochastic equation obtained for $\epsilon = 0$, and the properties of the fix-point distribution. Two examples for the convergence of the sampling algorithm (Figs. 17.3, 17.4) illustrate this dependence. First, take the non-stochastic fix-point equation $x = f(x)$ with $f(x) = x^3 - 1.25 \cdot x$. This equation has three fix-points $x_1 = 0$, $x_{2/3} = \pm 1.5$. All fix-points are instable, since the slope $|f'(x_i)|$, $i = 1, 2, 3$, is larger than 1. Direct iteration of $f(x)$ converges to the stable two-cycle ± 0.5, but misses the instable fix-point x_1. The usual trick to avoid two-cycles, namely rewriting the equation as $x = (x + f(x))/2$, results for starting values in $(-1.5, 1.5)$ in convergence to x_1, where the slope is negative. To check convergence of the sampling algorithm the fix-point equation is rewritten as a stochastic equation $x = F[x_1, \ldots, x_k] = f(\sum_{i=1}^{K} x_i/K)$, with identical fix-points. If we initialize the sample with values in $[0, 1]$ – any subset of $(-1.5, 1.5)$ would work – the distribution of x constructed in the sampling converges to a δ-peak at the fix-point $x_1 = 0$ of the original equation (see Fig. 17.3). As for this example, convergence of the sampling algorithm is generally better than for direct iteration of the original equation. This result should imply good convergence for (17.5). For $p(\epsilon_i) = \delta(\epsilon_i)$, i.e. without disorder, already direct iteration converges to the Green function $G^0(\omega)$ of the Bethe lattice, and sampling of the distribution is therefore expected to converge fairly well. Nevertheless, as the second example shows, convergence may worsen for the full stochastic equation even if it is pretty good for the non-stochastic one. For the second example we apply the sampling algorithm to the solution of (17.5) with disorder, i.e. $p(\epsilon_i) \neq \delta(\epsilon_i)$. While in the previous example the convergence to the fix-point distribution is very regular, the ϵ_i provide an explicit source of randomness which leads to fluctuations in the sample during

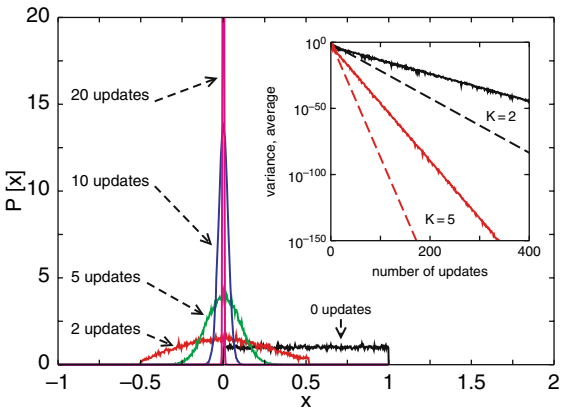

Fig. 17.3. Convergence of a distribution within the sampling algorithm. Solving the equation $x = f(x)$ with $f(x) = x^3 - 1.25 \cdot x$ as a stochastic equation with $K = 2$. The picture shows the distribution $P[x]$ of x after some updates of a sample with $N_s = 5 \times 10^4$ entries; the inset displays the arithmetic average (solid line) and variance (dashed line) of the sample for $K = 2$ and $K = 5$. The distribution converges to a δ-distribution at the fix-point $x_0 = 0$, although $|f'(x_0)| = 1.25 > 1$

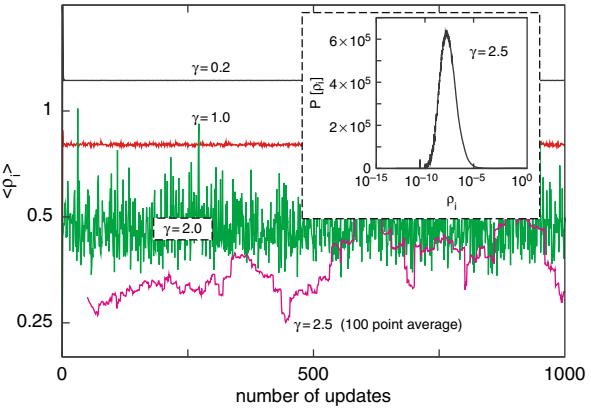

Fig. 17.4. Convergence of a distribution within the sampling algorithm. Fluctuations of the average $\langle\rho_i\rangle$ of the LDOS distribution $P[\rho_i(\omega)]$ to (17.5) during updates of a sample with $N_s = 5 \times 10^4$ entries. The disorder distribution $p(\epsilon_i)$ is taken from (17.10), and $\omega = 0$. The curves to $\gamma = 0.2$ and $\gamma = 1.0$ correspond to the distributions shown in Fig. 17.8. For $\gamma = 2.5$, the average of 100 consecutive updates is shown instead of $\langle\rho_i\rangle$ (the fluctuations of $\langle\rho_i\rangle$ would fill the picture). The inset displays $P[\rho_i(\omega)]$ for $\gamma = 2.5$. Note the logarithmic abscissa

sampling. In Fig. 17.4 we show the fluctuations of the average of the LDOS distribution $P[\rho_i(\omega)]$. The larger γ in this example, i.e. the larger the variance of ϵ_i, the stronger fluctuations are. This is not an artifact of the algorithm, but results unavoidably from the properties of the fix-point distribution. As the inset in Fig. 17.4 shows, the fix-point distribution has extremely large variance. Resolving this equation by a sample with a finite number of entries results in typical large fluctuations associated with the statistics of rare events. We will see below, that the strength of fluctuations may even diverge, which signals a phase transition (here, the Anderson transition from extended to localized states, see Sect. 17.2.1). With strong fluctuations, the algorithm does not converge even in an approximate sense, and a single sample is not a good representation of the distribution. To sample the full distribution we then have to use a large number of consecutive samples obtained in update step `(2)`.

Note that convergence in the first example has been faster for $K = 5$ than for $K = 2$. For (17.5) this observation implies that convergence becomes better with increasing K – just as one comes close to the limit $K = \infty$, where the stochastic equation can be replaced by one for averages.

17.2 Applications of the LD Approach

After the construction of the LD approach and the explanation of the Monte Carlo sampling we shall now discuss some results of the LD approach. In addition to the examples given here we also refer the reader to [10, 11, 12, 13]. For all examples,

we set $K = 2$ in (17.5), and measure energies in units of the bandwidth W (if we fix $W = 1$, $t = 1/\sqrt{32}$ for the $K = 2$-Bethe lattice).

17.2.1 Non-Interacting Disordered Systems

Let us begin with two examples of non-interacting disordered systems [14]. The first example is the binary alloy model, which describes a solid composed of two atomic species A, B. The on-site energies are distributed as

$$p(\epsilon_i) = c_A \delta(\epsilon_i + \Delta/2) + (1 - c_A)\delta(\epsilon_i - \Delta/2) \; , \tag{17.9}$$

where Δ is the separation of the energy levels of A,B atoms, and c_A ($c_B = 1 - c_A$) is the concentration of A (B) atoms.

At a first glance we should expect, for $\Delta > W$, two bands in the DOS centered at $\pm\Delta/2$, with weight c_A and $1 - c_A$ respectively. Indeed this is what we get by the CPA, if we solve (17.8). If we compare to the result obtained from the stochastic approach, solving (17.5) by the sampling algorithm, we find that the averaged CPA description misses important features of the alloy (see Fig. 17.5). Remember that the stochastic approach is exact in this situation: The DOS shown gives the true picture of the system.

Why does CPA fail in this case? Physically, the electron motion is strongly affected by multiple scattering on finite clusters of either A or B atoms, whereby the DOS develops a rich structure. The most prominent peaks in the DOS can be directly attributed to small clusters, as indicated in Fig. 17.5. For the parameters chosen here, the concentration c_A is below the classical percolation threshold, hence all clusters of the minority species A are finite. This is the origin of the fragmentation

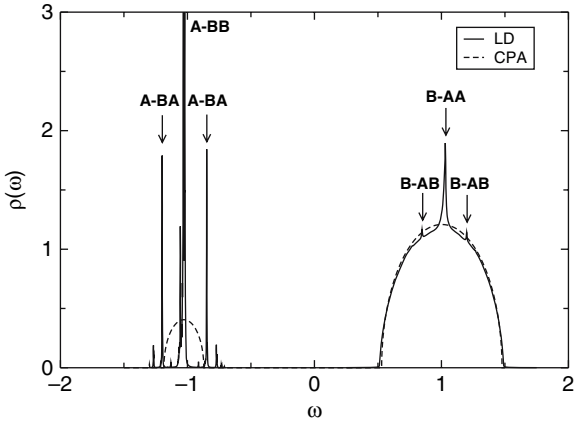

Fig. 17.5. DOS $\rho(\omega)$ for the binary alloy model, with $\Delta = 2.0$, $c_A = 0.1$. The picture shows both CPA and LD results. To resolve the δ-peaks in the minority band, the LD curve has been broadened by including an artificial imaginary part $\eta = 10^{-3}$ in the energy $\omega + \mathrm{i}\eta$. Arrows mark contributions from small finite clusters of atoms. Figure taken from [14]

of the minority A-band. CPA, being constructed in the limit $K \to \infty$, averages over spatial fluctuations and does therefore not properly account for multiple scattering. From the stochastic viewpoint, this is manifest in the LDOS distribution $P[\rho_i(\omega)]$ (see Fig. 17.6), which cannot be represented by a single value. Especially it is not senseful to replace $P[\rho_i(\omega)]$ by $\rho(\omega)$ as in the CPA.

The second example we consider is the Anderson model of localization, which assumes a box distribution of on-site energies

$$p(\epsilon_i) = \frac{1}{\gamma}\,\Theta(\frac{\gamma}{2} - |\epsilon_i|)\ , \tag{17.10}$$

with $\gamma \geq 0$ as the strength of disorder. In contrast to the binary alloy with its discrete distribution, the DOS in the Anderson model is well described by CPA, expect for some details at the band edges (see Fig. 17.7). But, invisible in the DOS, the character of states is different towards the band edges and in the band center, as could already be anticipated from Fig. 17.1. While states in the band center resemble distorted Bloch waves, which extend through the whole crystal, states towards the band edge have appreciable weight only in finite (separated) regions of the crystal. An electron in such a state is not itinerant any more, hence the state is called localized in contrast to extended Bloch-like states. As localized states do not contribute to the electrical conductivity, Anderson localization is a mechanism to drive a metal into an insulator as a result of disorder. While for interaction-driven metal-insulator transitions like the Mott or Peierls transition a gap in the DOS opens at the transition, the DOS stays finite at the Anderson transition from localized to extended states. It is only the conductivity which drops to zero.

Guided by our discussion of Fig. 17.1, one expects that localized and extended states can be distinguished by means of the LDOS distribution. Fig. 17.8 shows

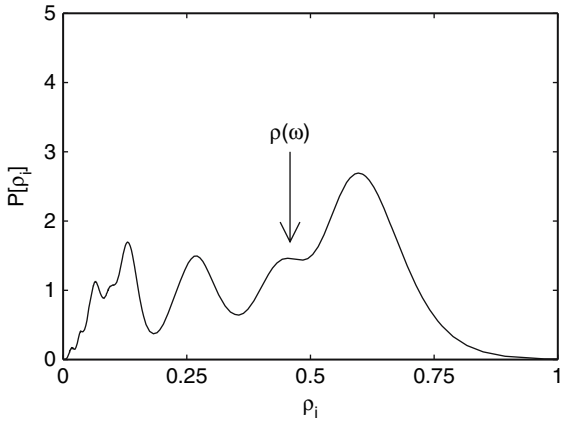

Fig. 17.6. LDOS distribution $P[\rho_i(\omega)]$ for the binary alloy model at $\omega = 0.0$, with $\Delta = 0.3$, $c_A = 0.1$. The arrow marks the DOS $\rho(\omega)$. Evidently a single value cannot represent the distribution in any sense

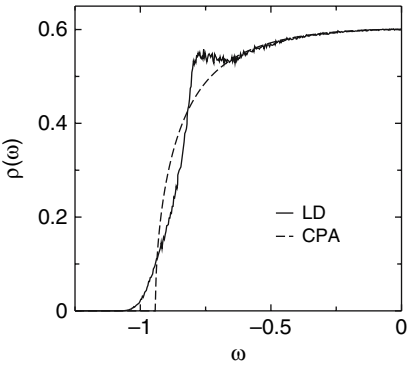

Fig. 17.7. DOS $\rho(\omega)$ for the Anderson model, at $\gamma = 1.5$. The picture shows both CPA and LD results. Since $\rho(-\omega) = \rho(\omega)$, only one half of the figure is shown. Note the sharp band edge within the CPA approximation, and the smooth *Lifshitz* tails in the LD result. These tails result from the exponentially few (localized) states at sites with large $|\epsilon_i|$ which are not resolved within CPA

$P[\rho_i(\omega)]$ for weak and moderate disorder. For weak disorder, the distribution resembles a Gaussian peaked at the (averaged) DOS $\rho(\omega)$. With increasing disorder, as fluctuations of the LDOS grow, the distribution becomes increasingly broad and asymmetric. The DOS is then not representative for the distribution anymore. With even increasing disorder, the distribution becomes singular at the transition to localized states: All but infinitesimally small weight resides at $\rho_i = 0$. This singularity in $P[\rho_i(\omega)]$ has to be accessed via analytical continuation of a Green function to the real axis, as is depicted in Fig. 17.9 Although the distribution becomes singular at the localization transition, the DOS is nevertheless still finite due to negligible

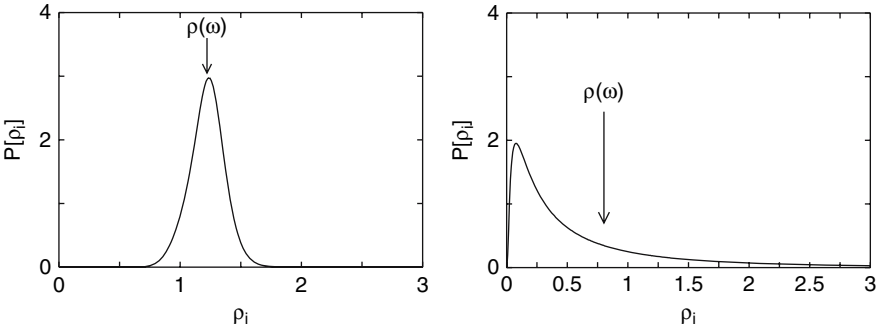

Fig. 17.8. LDOS distribution $P[\rho_i(\omega)]$ for the Anderson model, in the band center $\omega = 0$. The arrows mark the DOS $\rho(\omega)$. Left: For weak disorder $\gamma = 0.2$, the distribution is peaked at the $\rho(\omega)$. Right: Already for moderate disorder $\gamma = 1.0$, the DOS is not significant for the distribution, which is very skew and broad. Compare this to the distribution shown in Fig. 17.4 for even stronger disorder

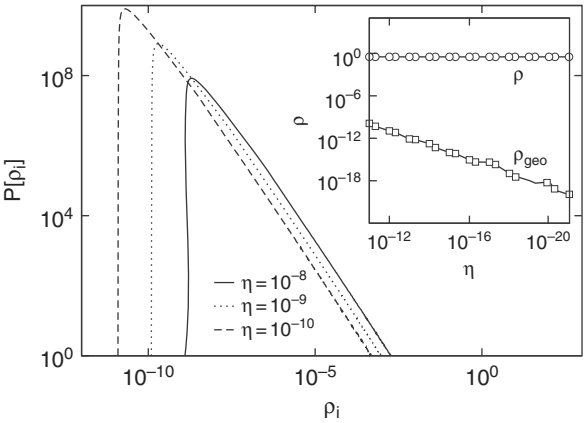

Fig. 17.9. The figure shows, how $P[\rho_i(\omega)]$ for localized states in the Anderson model depends on the imaginary part η in the energy argument of the Green function $G_i(\omega + \mathrm{i}\eta)$. For $\eta \to 0$, numerically performing analytical continuation to the real axis, the DOS $\rho(\omega)$ stays finite, but a typical moment, like the geometrically averaged LDOS $\rho_{\mathrm{geo}}(\omega)$, goes to zero

weight at infinitely large values of $\rho_i(\omega)$. Anderson localization therefore manifests itself in the full distribution $P[\rho_i(\omega)]$ but not in an averaged value like $\rho(\omega)$. As for the binary alloy, a description in averages is prevented by the pronounced spatial fluctuations which constitute localization.

To obtain the phase diagram of the Anderson model (Fig. 17.10) which shows the transition line between localized and extended states – the so-called mobility edge –, we employ the above criterion based on the LDOS distribution. Since the DOS does not indicate Anderson localization, the phase diagram could not be obtained from CPA. Indeed, as should be apparent from our discussion, CPA misses localization at all. Looking at the distributions, we can expect CPA to describe the system well only for small disorder and away from the band edges, when $P[\rho_i(\omega)]$ is peaked at $\rho_i(\omega)$ (left panel in Fig. 17.8). There, an electron propagates diffusively, and correlations in the electron motion are weak. There is however no simple way to extend an averaged theory like CPA to all disorder strengths or energies.

We should mention that localization also occurs in the binary alloy model. For small enough c_A and large Δ (see Fig. 17.11 for the DOS), when all A-clusters are finite and scattering on interlying B-atoms is strong, one expects that all states in the A-band are localized. Tunneling processes between separated A-clusters may nevertheless give rise to extended states. For the parameters in Fig. 17.5 states in the A-band are localized. The DOS then consists of a series of δ-peaks which had to be broadened with some finite η to be seen in the picture. Note that for the Anderson model the δ-peaks densely fill the energy regime of localized states – a so-called Dirac comb or dense pure point spectrum in mathematical terms. The DOS of the Anderson model is therefore smooth, while for the binary alloy the tendency to gap formation prevails. This is a precursor of percolative behavior for $\Delta \to \infty$.

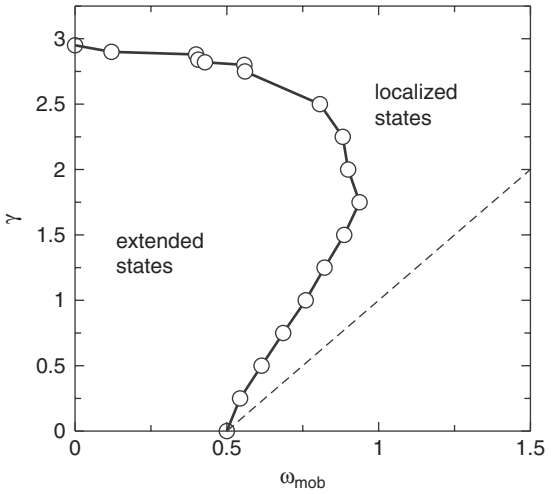

Fig. 17.10. Phase diagram of the Anderson model. Shown is the mobility edge ω_{mob} vs. γ. The dashed line shows the exact band edge $\omega = (W + \gamma)/2$. The trajectory is symmetric under $\omega_{\mathrm{mob}} \mapsto -\omega_{\mathrm{mob}}$. Note that for small γ, ω_{mob} grows before it tends to zero when γ approaches the critical value for complete localization (so-called re-entrant behavior)

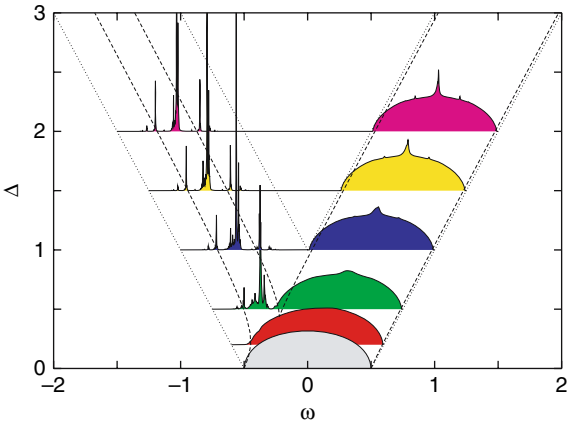

Fig. 17.11. Part of a phase diagram of the binary alloy model for concentration $c_A = 0.1$, showing the DOS for various Δ. The dashed curves show the CPA band edges, the dotted lines mark $\omega = \pm\Delta/2 \pm W/2$. Figure taken from [14]

17.2.2 Extension to Interacting Disordered Systems

Within DMFT, interaction properties are subsumed in a $\boldsymbol{k}$-independent self-energy $\Sigma(\omega)$. Transforming to real space, we get a local self-energy $\Sigma_{ii}(\omega)$, which however does not depend on the lattice site i for ordered systems. The LD approach rests on the observation, that in the presence of disorder previously site-independent quantities become site-dependent. This applies not only to the local Green function $G_{ii}(\omega)$ but also to the self-energy $\Sigma_{ii}(\omega)$. In order to extend the LD approach to interacting systems – or the DMFT to disordered ones – one has to introduce a site-dependent self-energy $\Sigma_{ii}(\omega)$, which can be understood as a random variable like the Green function $G_{ii}(\omega)$ [13].

Remember that in DMFT $\Sigma_{ii}(\omega)$ with $G_{ii}(\omega) = G^0_{ii}(\omega - \Sigma_{ii}(\omega))$ is obtained from the solution of an Anderson impurity problem, in dependence on a local propagator

$$\mathcal{G}_{ii}(\omega) = \left[G_{ii}(\omega)^{-1} + \Sigma_{ii}(\omega)\right]^{-1} , \tag{17.11}$$

which excludes interaction at site i. Formally, $\Sigma_{ii}(\omega)$ is a functional of $\mathcal{G}_{ii}(\omega)$,

$$\Sigma_{ii}(\omega) = \Sigma_{ii}[\mathcal{G}_{ii}(\omega)] , \tag{17.12}$$

whose explicit form is not known in most cases. For the Bethe lattice with its semicircular DOS, simple expressions for $\mathcal{G}_i(\omega)$ and $G_i(\omega)$ exist, namely

$$\begin{aligned} \mathcal{G}_i(\omega) &= \Big[\omega - \epsilon_i - t^2 \sum_{j=1}^{K} G_j(\omega)\Big]^{-1} , \\ G_i(\omega) &= \left[\mathcal{G}_i(\omega)^{-1} - \Sigma_i(\omega)\right]^{-1} \\ &= \Big[\omega - \epsilon_i - \Sigma_i(\omega) - t^2 \sum_{j=1}^{K} \mathcal{G}_j(\omega)\Big]^{-1} , \end{aligned} \tag{17.13}$$

– this is of course just the equivalent to (17.5) – while the complexity of (17.12) does not reduce a single bit. Clearly, with the Green function $G_{ii}(\omega)$ also the self-energy $\Sigma_{ii}(\omega)$ is a random quantity. The Equations (17.11)–(17.13) therefore have the same status in an interacting system as (17.5) has without interaction: They form stochastic self-consistency equations for $\Sigma_{ii}(\omega)$ and $G_{ii}(\omega)$. Again, what would be an infinite number of coupled equations for self-energies and Green functions, reduces to few self-consistency equations if reformulated by means of distributions.

Solving these equations by Monte Carlo sampling the impurity problem (17.12) has to be solved in each update step `(2c)`. This constitutes the main part of the high computational complexity of the combined LD+DMFT approach. While in DMFT one has to solve the impurity problem some times till convergence, it has to be solved here repeatedly for each entry of the sample. The computational effort is therefore at least N_s times larger than in DMFT.

In few cases the DMFT impurity problem can be solved exactly. With an explicit solution for (17.12) at hand, the numerical effort to perform the sampling of

$G_i(\omega)$ can be handled. One example is the single polaron Holstein model [15] with Hamiltonian

$$H = -t \sum_{\langle i,j \rangle} c_i^\dagger c_j - \sqrt{\varepsilon_p \omega_0} \sum_i (b_i^\dagger + b_i) c_i^\dagger c_i + \omega_0 \sum_i b_i^\dagger b_i \ , \tag{17.14}$$

where an electron is coupled to optical phonons of energy ω_0. For this model, $\Sigma_i(\omega)$ is obtained as an infinite continued fraction [16]

$$\Sigma_i(\omega) = \cfrac{1\varepsilon_p\omega_0}{[\mathcal{G}_i(\omega - 1\omega_0)]^{-1} - \cfrac{2\varepsilon_p\omega_0}{[\mathcal{G}_i(\omega - 2\omega_0)]^{-1} - \cfrac{3\varepsilon_p\omega_0}{\cdots}}} \ . \tag{17.15}$$

The continued fraction is an expansion in terms of the maximal number of virtual phonons that are excited at the same time. Evidently, this expansion is non-perturbative, and contains diagrams of arbitrary order at any truncation depth of the fraction.

To give an impression of the physical content of the Holstein model, we show in Fig. 17.12 the DOS $\rho(\omega)$ in the anti-adiabatic (i.e. for large ω_0) strong coupling regime as obtained from a DMFT calculation based on (17.15). This picture illustrates the formation of a new quasi-particle which is a compound object of an

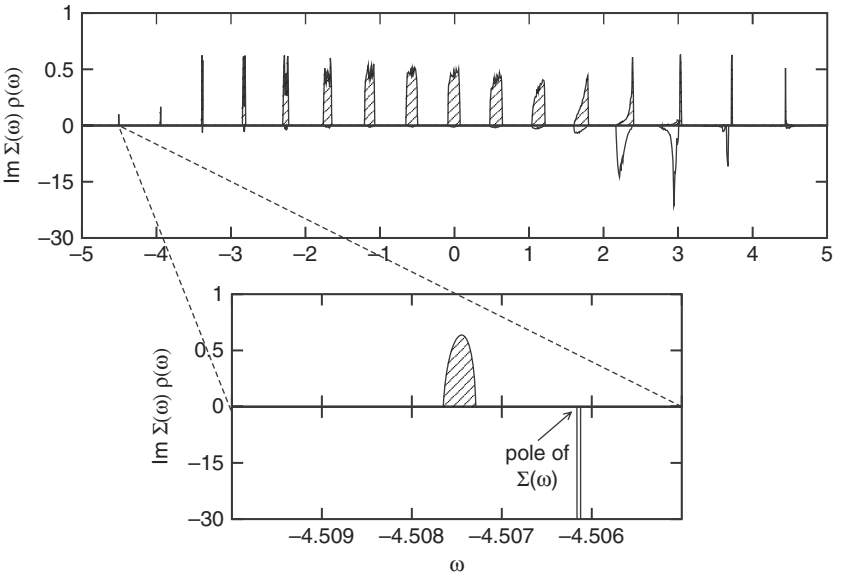

Fig. 17.12. The Holstein polaron at strong coupling and large phonon frequency. We show the DOS for the Holstein model with $\omega_0/W = 0.5625$, $\varepsilon_p/W = 4.5$. The center of the lowest sub-band is located nearly at $-\varepsilon_p$ (the polaron shift), and bands are separated by ω_0. The bandwidth of the lowest sub-band, which is shown in detail in the lower panel, is $W_{\text{sub}} = 3.45 \times 10^{-4} W$

electron with a surrounding cloud of phonons. This so-called small polaron is characterized by an extremely large mass resulting in a narrow quasi-particle band (in Fig. 17.12 the effective mass of the polaron is four orders of magnitude larger than the free electron mass). Note that, while the lowest polaron is fully coherent, as an effect of inelastic electron-phonon interaction higher bands are incoherent. Accordingly, the imaginary part of the self-energy is finite. The reader should be aware that the properties of the polaron intimately depend on the parameter values. Here we do by no means provide a general picture of polaron physics. For detailed discussions see e.g. [17, 18, 19], for a DMFT study of small polarons [20].

If the Hamiltonians (17.1) and (17.14) are combined, we obtain a model to study possible effects of Anderson localization of a polaron. Like for the polaron itself, the physics of polaron localization is diverse and complicated. A general discussion, as partly given in [21], is far beyond the scope of this tutorial. For the parameters used in Fig. 17.12 however, the polaron in its lowest band is a small and heavy quasi-particle with infinite lifetime. We therefore expect that disorder affects this quasi-particle like a free electron, but with the mass of the polaron. We can scrutinize this expectation within the LD+DMFT approach, which provides the mobility edge trajectory for the lowest sub-band (Fig. 17.13). Rescaling the trajectory properly it perfectly matches the trajectory of the Anderson model in Fig. 17.10. As a fundamental observation we note that the critical disorder for complete localization of all states in the polaron sub-band is renormalized by W_{sub}/W as compared to the free electron: In any real material such a polaron would be localized for almost arbitrarily small disorder.

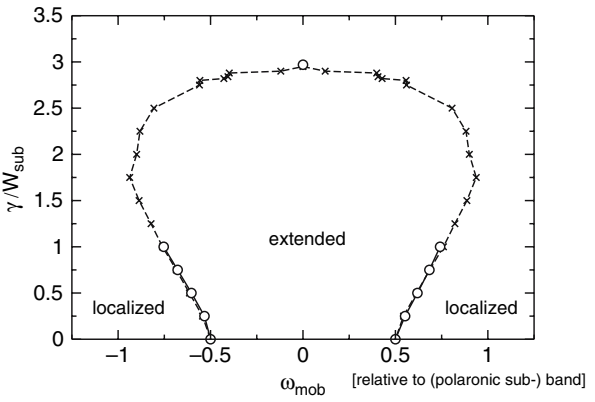

Fig. 17.13. Phase diagram for Anderson localization of a Holstein polaron at strong coupling and large phonon frequency. As in the previous figure, $\omega_0/W = 0.5625$, $\varepsilon_p/W = 4.5$. Shown is the mobility edge for the lowest polaronic sub-band (*circles*) in comparison to the Anderson model for a free electron (*crosses*). γ and ω_{mob} is rescaled to the respective bandwidth. The energy scale of both curves accordingly differs by almost four orders of magnitude, as $W_{\text{sub}} = 3.45 \times 10^{-4} W$

To avoid any misconception we like to point out that polaron localization in this example shows up as renormalization of e.g. the critical disorder only for the reason that the polaron here is a small quasi-particle with infinite lifetime. If the polaron would extend over some lattice sites, disorder would affect the structure of the polaron itself, instead of affecting the polaron as a compound entity. Likewise, if the quasi-particle lifetime is finite localization is weakened since the motion of the particle is incoherent then. This is already expressed by the fact that Anderson localization can only be detected in the limit $\eta \to 0$, as discussed before. Incidentally, the band fragmentation we saw in the minority band of the binary alloy is not destroyed by damping since finite gaps exist there. Remember that the latter one shows up in the DOS for finite η, while the former one shows up only in the distribution for $\eta \to 0$.

17.2.3 The Holstein Model at Finite Temperature

In the previous section we addressed the Holstein model at zero temperature, and imposed spatial fluctuations by disorder. But even without disorder, the physics of the Holstein model (17.14) may be strongly influenced by static scattering off spatial fluctuations. As mentioned in the introduction, this is the case for heavy ions, i.e. small oscillator frequency ω_0, when ions act as static scatterers to first order. If at finite temperature ions are displaced from their equilibrium positions, the concomitant random potential acts as a static disorder potential to first order (see also [19]).

Let us consider the limit of large ionic mass M, keeping the spring constant $k_s = M\omega_0^2$ of the harmonic oscillator $\omega_0 b_i^\dagger b_i$ constant. This limit, the so-called adiabatic limit $\omega_0 \to 0$ of small phonon frequency, is opposite to the regime of large phonon frequency to which the example from the previous section (Fig. 17.12) belongs. In the limit $\omega_0 \to 0$ ions are nearly classical particles. Classical states in the context of the harmonic oscillator can be constructed as coherent states $|\alpha\rangle$. Remember that a coherent states is a Gaussian wavepacket centered at $\bar{X}_i^\alpha = \langle\alpha|X_i|\alpha\rangle = \sqrt{2/(M\omega_0)}\,\mathrm{Re}\;\alpha$, with the position operator $X_i = \sqrt{1/(2M\omega_0)}(b_i + b_i^\dagger)$.

It is not difficult to convince oneself, that the thermal (Boltzmann) trace over boson eigenstates $|n\rangle$ can be expressed as an integral over coherent states:

$$\mathrm{Tr}_\beta[\ldots] = \frac{1}{2}\sum_{n=0}^{\infty} \mathrm{e}^{-\beta n\omega_0}\langle n|\ldots|n\rangle = \frac{\mathrm{e}^{\beta\omega_0}-1}{\pi}\int \mathrm{d}^2\alpha\; \mathrm{e}^{(1-\exp(\beta\omega_0))|\alpha|^2}\langle\alpha|\ldots|\alpha\rangle. \tag{17.16}$$

In the spirit of Monte Carlo integration the complex plane integral $\int \mathrm{d}^2\alpha \ldots$ has a stochastic counterpart: The integral value is obtained by sampling the expectation value $\langle\alpha|\ldots|\alpha\rangle$ for a complex random variable α with Gaussian probability density $\propto \exp[(1-\exp(\beta\omega_0))|\alpha|^2]$. This results in a stochastic interpretation of the Holstein model at finite temperature. The random part of the model is the initial state of the bosonic subspace, given by random coherent states $|\alpha_i\rangle$ at site i according to the specific distribution for α_i. The bosonic vacuum at $T = 0$ is therefore replaced by a fluctuating vacuum, where the strength of fluctuations depends on T.

From a local point of view as in the previous section, we need the Green function $G_i^\alpha(\omega)$, which in contrast to the Holstein model at $T = 0$ is not evaluated in the bosonic vacuum but within a certain coherent state $|\alpha_i\rangle$. The Green function is given by

$$G_i^\alpha(\omega) = \left[\mathcal{G}_i(\omega)^{-1} - \sqrt{2\varepsilon_p k_s}\bar{X}_i^\alpha - \Sigma_i^\alpha(\omega)\right]^{-1} . \tag{17.17}$$

This expression is of the same type as (17.13), with a static disorder contribution given by the random variable $\bar{X}_i^\alpha$, and a self-energy contribution $\Sigma_i^\alpha(\omega)$ accounting for finite lifetime effects, i.e. finite ω_0. Note that $\sqrt{\varepsilon_p}\bar{X}_i^\alpha$, being an effect of interaction, enters $G_i^\alpha(\omega)$ but not $\mathcal{G}_i(\omega)$. $\bar{X}_i^\alpha$ has Gaussian distribution $P[\bar{X}_i^\alpha] \propto \exp[(1 - \exp(\beta\omega_0))M\omega_0(\bar{X}_i^\alpha)^2/2]$ resulting from (17.16). Both for high temperature ($\beta \to 0$) and in the adiabatic limit ($\omega_0 \to 0$), the classical result $P[\bar{X}_i^\alpha] \propto \exp[-\beta k_s(\bar{X}_i^\alpha)^2/2]$ is obtained. Note that the Green function $G_i^\alpha(\omega)$ is evaluated in bosonic states that are not eigenstates of the bosonic number operator $b_i^\dagger b_i$, and therefore in principle is a non-equilibrium Green function with different analytical properties as retarded Green functions $G_i(\omega)$ used elsewhere in the text. On average however, i.e. for the disorder averaged Green function $\langle G_i^\alpha \rangle$ which is obtained as the average over α_i instead of ϵ_i as in the previous sections, the full analytical properties of a retarded Green function are recovered.

The self-energy $\Sigma_i^\alpha(\omega)$ can be expressed as a continued fraction like for the Holstein model at zero temperature. The expression is derived at considerably less ease than before – e.g. using Mori-Zwanzig projection techniques [22] – and acquires a less systematic form. From the top level of the continued fraction,

$$\Sigma_i^\alpha(\omega) = \cfrac{\omega_0(\varepsilon_p - 2\mathrm{i}\sqrt{\varepsilon_p\omega_0}\ \mathrm{Im}\,\alpha_i)}{\omega - \cfrac{2\sqrt{\varepsilon_p\omega_0}(\varepsilon_p + \omega_0)\,\mathrm{Re}\,\alpha_i + \varepsilon_p\omega_0(1 - 4\mathrm{i}\,\mathrm{Re}\,\alpha_i\ \mathrm{Im}\,\alpha_i)}{\varepsilon_p - 2\mathrm{i}\sqrt{\varepsilon_p\omega_0}\ \mathrm{Im}\,\alpha_i} - \dots} \tag{17.18}$$

we deduce that $\Sigma_i^\alpha(\omega)$ is of order ω_0, while $\bar{X}_i^\alpha$ is of order 1. The expression for $G_i^\alpha(\omega)$ therefore acquires the correct form as an expansion in ω_0. Note that (17.16)–(17.18) hold for any parameters values, but are constructed to work in the limit of small ω_0. The continued fraction (17.15), which is straightforwardly generalized to arbitrary eigenstates $|n\rangle$ of $b^\dagger b$, is not applicable in this case: For $\omega_0 \to 0$ the number of bosons in the thermal trace becomes large, which renders an expansion in the number of excited bosons useless.

By (17.16)–(17.18) the Holstein model for small $\omega_0 \to 0$ and finite T is cast in a form that is amenable to the stochastic method explicated in the preceding sections. Here, we do not supply actual calculations based on that. The bottom line instead is the interpretation provided by our reformulation: Temperature induced spatial fluctuations act to a certain degree like (static) disorder. In (17.17) the main source of resistivity due to scattering off thermally excited phonons is translated to disorder scattering: With increasing T, the amount of fluctuations of the disorder potential $\sqrt{\varepsilon_p k_s}\bar{X}_i^\alpha$ increases, and electron motion is strongly suppressed. We know from disordered systems that the suppression is much larger than expected from

first estimates based on uncorrelated scattering, which neglect correlations in the electron motion which eventually lead to Anderson localization. Will an electron subject to electron-phonon interaction ever be localized at finite T? Exactly for $\omega_0 = 0$, with $\Sigma_i^\alpha = 0$, we end up with a disorder problem, and localization can occur. But otherwise, surely not: For any $\omega_0 \neq 0$ the ionic potential seen by an electron is not static but changes on a timescale $\propto 1/\omega_0$. Anderson localization itself is then suppressed by incoherent scattering where the electron exchanges energy with ions, e.g. by absorption of thermally excited phonons.[6] Nevertheless strong suppression of electron transport at small ω_0 exists as a precursor of Anderson localization.

17.3 Summary

At the end of this tutorial we shall return to the initial question we raised: How to set up a kind of mean-field theory for spatial fluctuations and correlations. The essential idea argued for is to adopt a stochastic viewpoint: The mean-field in the theory has to be the distribution of a certain quantity – that is a stochastic mean-field theory which does not have a *mean*-field at all. We first had to convince ourselves – taking disordered systems as the example for fluctuations of a potential in space – that important quantities like the density of states are indeed best understood as random quantities which should be described by their distribution. The main effort was to construct a working scheme, the LD approach, out of this basic premise of the stochastic viewpoint. Technically that included the derivation of a closed set of stochastic equations for the distribution of the local density of states as the quantity of interest. In the derivation a complicated set of equations could be collapsed into a single equation if formulated with the help of distributions. For the solution of this stochastic equation we discussed the application of Monte Carlo sampling.

As much as we used disordered systems to motivate the central concepts leading to the LD approach we took them as the first example to demonstrate its application. Notably, even a complex non-local effect like Anderson localization is correctly described by distributions of a local quantity. This demonstrates how correlations turn up in local distributions. On the other hand we had to accept that a disordered system is always far from the limit $d = \infty$. Both the second example – Anderson localization of a Holstein polaron as an interacting disordered system – and the third example – the Holstein model at finite temperature – show that we generally cannot separate temporal fluctuations from spatial ones. The competition between the different physical mechanism present in these problems gives rise to very rich physical behavior. The central features of such systems become accessible only within a theory which accounts for both spatial and temporal fluctuations on an equal footing, as the combined LD+DMFT approach does.

[6] Remember the discussion in the previous section concerning the case of large ω_0, opposite to the adiabatic limit addressed here. There we noted that only in a coherent polaron band Anderson localization affects a polaron like a free – albeit heavy – particle.

There is a number of (open) questions we could not touch upon here. The calculation of transport properties is one important example, which is not really understood at the present stage of development. Taking the Holstein model at finite temperature as an example, we sketched how to address the issue of transport at $T > 0$ in the notoriously difficult limit of small ω_0 by means of a stochastic formulation. To actually resolve this issue within the LD approach we have to specify a way how to obtain the electric conductivity from local distributions, aside from the need to actually perform the numerical calculations. There is no definite answer yet, which is ready to be implemented. We nevertheless believe to have given arguments that thinking in terms of distributions can prove worthwhile also here. Maybe we should rephrase our introductory word of warning concerning the content of this tutorial: It's not just about a method, it's about a way of thinking!

References

1. N.W. Ashcroft, N.D. Mermin, *Solid State Physics* (Saunders College Publ., Philadelphia, 1976) 505
2. J. Hubbard, Phys. Rev. Lett. **3**, 77 (1959) 505
3. R.L. Stratonovich, Dokl. Akad. Nauk SSSR **115**, 1097 (1957) 505
4. A. Georges, G. Kotliar, W. Krauth, M.J. Rozenberg, Rev. Mod. Phys. **68**, 13 (1996) 505
5. P.W. Anderson, Phys. Rev. **109**, 1492 (1958) 506
6. R.J. Elliot, J.A. Krumhansl, P.L. Leath, Rev. Mod. Phys. **46**, 465 (1974) 506, 511
7. P.A. Lee, T.V. Ramakrishnan, Rev. Mod. Phys. **57**, 287 (1985) 506
8. B. Kramer, A. Mac Kinnon, Rep. Prog. Phys. **56**, 1469 (1993) 506
9. R. Abou-Chacra, D.J. Thouless, P.W. Anderson, J. Phys. C **6**, 1734 (1973) 509
10. S.M. Girvin, M. Jonson, Phys. Rev. B **22**, 3583 (1980) 514
11. D.E. Logan, P.G. Wolynes, Phys. Rev. B **29**, 6560 (1984) 514
12. D.E. Logan, P.G. Wolynes, Phys. Rev. B **36**, 4135 (1987) 514
13. V. Dobrosavljević, G. Kotliar, Philos. Trans. Roy. Soc. Lond., Ser. A **356**, 57 (1998) 514, 520
14. A. Alvermann, H. Fehske, Eur. Phys. J. B **48**, 205 (2005) 515, 519
15. T. Holstein, Ann. Phys. (N.Y.) **8**, 343 (1959) 521
16. H. Sumi, J. Phys. Soc. Jpn. **36**, 770 (1974) 521
17. Y.A. Firsov, *Polarons* (Izd. Nauka, Moscow, 1975) 522
18. H. Fehske, A. Alvermann, M. Hohenadler, G. Wellein, in *Polarons in Bulk Materials and Systems With Reduced Dimensionality*, *International School of Physics Enrico Fermi*, Vol. 161, ed. by G. Iadonisi, J. Ranninger, G. De Filippis (IOS Press, Amsterdam, 2006), *International School of Physics Enrico Fermi*, Vol. 161, pp. 285–296 522
19. H. Fehske and S.A. Trugman in *Polarons in Advanced Materials*, Ed. A.S. Alexandrov, Springer Series in Material Sciences Vol. 103, pp. 393–461 (Canopus/Springer, Dordrecht 2007) 522, 523
20. S. Ciuchi, F. de Pasquale, S. Fratini, D. Feinberg, Phys. Rev. B **56**, 4494 (1997) 522
21. F.X. Bronold, A. Alvermann, H. Fehske, Philos. Mag. **84**, 673 (2004) 522
22. P. Fulde, *Electron Correlation in Molecules and Solids* (Springer-Verlag, Berlin, 1991) 524